

AN ITERATIVE SOLVER FOR THE HPS DISCRETIZATION APPLIED TO THREE DIMENSIONAL HELMHOLTZ PROBLEMS *

JOSÉ PABLO LUCERO LORCA [†], NATALIE BEAMS , DAMIEN BEECROFT , AND ADRIANNA GILLMAN [‡]

Abstract. This manuscript presents an efficient solver for the linear system that arises from the Hierarchical Poincaré-Steklov (HPS) discretization of three dimensional variable coefficient Helmholtz problems. Previous work on the HPS method has tied it with a direct solver. This work is the first efficient iterative solver for the linear system that results from the HPS discretization. The solution technique utilizes GMRES coupled with an exact block-Jacobi preconditioner. The construction of the block-Jacobi preconditioner involves two nested local solves that are accelerated by local homogenization. The local nature of the discretization and preconditioner naturally yield matrix-free application of the linear system. A distributed memory implementation allows the solution technique to tackle problems approximately 50 wavelengths in each direction requiring more than a billion unknowns to get approximately 7 digits of accuracy in less than an hour. Additional numerical results illustrate the performance of the solution technique.

Key words. Helmholtz, HPS, block-Jacobi, Domain Decomposition, Poincaré-Steklov, GMRES.
AMS subject classifications. 65N22, 65N35, 65N55, 65F05

1. Introduction. Consider the variable coefficient Helmholtz problem with impedance boundary conditions given below

$$(1.1) \quad \begin{aligned} -\Delta u(\mathbf{x}) - \kappa^2(1 - b(\mathbf{x}))u(\mathbf{x}) &= s(\mathbf{x}), & \mathbf{x} \in \Omega, \text{ and} \\ \frac{\partial u}{\partial n} + i\eta u(\mathbf{x}) &= t(\mathbf{x}), & \mathbf{x} \in \partial\Omega. \end{aligned}$$

where $\Omega = (0, 1)^3 \subset \mathbb{R}^3$, $u(\mathbf{x}) : \Omega \rightarrow \mathbb{C}$ is the unknown solution, $\kappa \in \mathbb{R}$ is the so-called *wave number*, $b(\mathbf{x}) : \Omega \rightarrow \mathbb{C}$ is a given smooth scattering potential and n is the outward normal unit vector to the boundary of the domain. The functions $s(\mathbf{x}) : \Omega \rightarrow \mathbb{C}$ and $t(\mathbf{x}) : \partial\Omega \rightarrow \mathbb{C}$ are assumed to be smooth functions.

This manuscript presents an efficient technique for solving the linear system that stems from the discretization of (1.1) with the Hierarchical Poincaré-Steklov (HPS) method. Roughly speaking the HPS method is a discretization technique based on local “element”-wise spectral collocation. Continuity of the solution and the flux are enforced at the interface between elements via a Poincaré-Steklov operator. In the case of the Helmholtz equation, this operator is the Impedance-to-Impedance (ItI) operator. As with other element-wise discretization techniques, the matrix that results from the HPS is sparse where all non-zero entries correspond to an element acting on itself or with a neighbor. Such sparse matrices can be applied in the so-called *matrix-free* format which means that the matrix can be applied by sweeping over the elements and never building the full matrix.

The efficient solution for the linear system resulting from the HPS discretization presented in this paper utilizes a block Jacobi preconditioned GMRES [22] solver. The application of the proposed block Jacobi preconditioner and the matrix itself are applied via matrix-free operations and exploit the tensor product nature of the element

*Submitted to the editors 3 December 2021.

Funding: This work was funded by Total Energies and NSF.

[†]Department of Applied Mathematics, University of Colorado at Boulder (pablo.lucero@colorado.edu, <https://pablo.lucero/math>).

[‡]Department of Applied Mathematics, University of Colorado at Boulder (adrianna.gillman@colorado.edu, <https://www.colorado.edu/amath/adrianna-gillman>).

wise discretization matrices. The proposed preconditioner requires the exact inversion of the Jacobi blocks which are accelerated by local homogenization at the element level. The local nature of the blocks and the preconditioner make the solution technique naturally parallelizable in a distributed memory model. Numerical tests show that the solution technique is efficient and capable of tackling problems with a billion degrees of freedom in less than forty minutes in parallel.

1.1. Prior work on the HPS method. The HPS method is a recently developed discretization technique [7, 11, 13, 14, 15, 19], based on local spectral collocation where the continuity of the solution and the flux is enforced via Poincaré-Steklov operators. For general elliptic problems, it is sufficient enough to use the Dirichlet-to-Neumann operator [18, Rem. 3.1]. For Helmholtz problems, the Impedance-to-Impedance (ItI) operator is used. By using this unitary operator for the coupling of elements, the HPS method is able to avoid artificial resonances and does not appear to observe the so-called *pollution effect* [13]. The paper [8] provides some analysis supporting the numerical results seen in practice.

Remark 1.1. Roughly speaking, pollution [1, Def. 2.3] is the need to increase the number of degrees of freedom per wavelength as the wave number κ grows in order to maintain a prescribed accuracy. This problem is known to happen when Galerkin finite element discretizations in two and more space dimensions are applied to Helmholtz problems [1, 2, 6].

Thus far the HPS method has only been applied to problems when coupled with a nested dissection [12] type direct solver. For two dimensional problems, this direct solver is easily parallelizable [7] and integrated into an adaptive version of the discretization technique [11]. Additionally, the computational cost of the direct solver is $O(N^{3/2})$, where N is the number of discretization points, for two dimensional problems with a small constant. For many problems the direct solver can be accelerated to have a computational cost that scales linearly with respect N in two dimensions [14] and $O(N^{4/3})$ in three dimensions [15]. This manuscript presents the first iterative solution technique for the linear system that arises from the HPS discretization.

1.2. Related work. There are several spectral collocation techniques that are similar to the HPS discretization in spirit (such as [20]). A thorough review of those methods is provided in [19].

The block Jacobi preconditioner presented in this paper can be viewed as a non-overlapping Schwarz domain decomposition preconditioner. Domain decomposition preconditioned solvers are widely used for solving large PDE discretizations with a distributed memory model parallelization. These techniques rely on the algorithm being able to perform the bulk of the calculation *locally* in each subdomain and limiting the amount of communication between parallel processes (see [24, 25] and references therein). Whenever possible using local tensor product formulations for the discretized operator and preconditioner, matrix-free techniques can accelerate the implementation and minimize memory footprint of domain decomposition preconditioned solvers (e.g. [16, 17]). By using a high order Chebyshev tensor product local discretization and sparse inter-element operators, the techniques presented in this manuscript are domain decomposing in nature and their implementation matrix-free to a large extent.

The implementation of the algorithms presented in this paper are parallelized using the PETSC library [3, 4, 5] with a distributed memory model.

1.3. Outline. The manuscript begins by describing the HPS discretization (in section 2) and how the linear system that results from that discretization can be

applied efficiently in a matrix-free manner in section 3. Then section 4 presents the proposed solution technique, including a block Jacobi preconditioner and its fast application. Next section 5 presents the technique for implementing the solver on a distributed memory platform. Numerical results illustrating the performance of the solver are presented in section 6. Finally, the paper concludes with a summary highlighting the key features and the impact of the numerical results.

2. Discretizing via the HPS method. The HPS method applied to (1.1) is based on partitioning the geometry Ω into a collection of small boxes of the same size. In previous papers on the HPS method, these small boxes have been called *leaf* boxes but the term *element* from the finite element literature can also be applied to them. Each element is discretized with a modified spectral collocation method and continuity of impedance data is used to *glue* the boxes together. This section reviews the discretization technique and presents an efficient and a *matrix-free* way of applying the matrix that results from the discretization.

Remark 2.1. This manuscript considers a uniform mesh or domain partitioning for simplicity of presentation. The technique can easily be extended to a nonuniform mesh with the use of interpolation operators and maintaining the appropriate ratio in size between neighboring boxes (as presented in [11]).

2.1. Leaf discretization. This section describes the discretization technique that is applied to each of the leaf boxes. This corresponds to locally discretizing with a modified classical spectral collocation technique the differential equation (1.1) with a fictitious impedance boundary condition on each leaf box. The modified spectral collocation technique was first presented in [11] for two dimensional problems.

Consider the leaf box (or element) $\Omega^\tau \subset \Omega$. The modified spectral collocation technique begins with the classic $n_c \times n_c \times n_c$ tensor product Chebyshev grid and the corresponding standard differentiation matrices \tilde{D}_x , \tilde{D}_y and \tilde{D}_z , as defined in [9, 26], on Ω^τ . Here n_c denotes the number of Chebyshev nodes in one direction. The entries of \tilde{D}_x , \tilde{D}_y and \tilde{D}_z corresponding to the interaction of the corner and edge points with the points on the interior of Ω^τ are zero thanks to the tensor product basis. Thus we can safely remove these discretization nodes and define D_x , D_y and D_z as the submatrices of \tilde{D}_x , \tilde{D}_y and \tilde{D}_z that approximate the derivatives of functions with a basis that does not have interpolation nodes at the corner and edge points entries.

Based on a tensor product grid without corner and edge points, let I_i^τ denote the index vector corresponding to points in the interior of Ω^τ and I_b^τ denote the index vector corresponding to points on the faces at the boundary of Ω^τ . Figure 2.1 illustrates this local ordering on a leaf box with $n_c = 10$. Let n , n_b and n_i denote the number of discretization points on a leaf box, the number of discretization points on the boundary of a leaf box and the number of discretization points in the interior of a leaf box, respectively. Then $n = n_i + n_b$. For three-dimensional problems $n_i = (n_c - 2)^3$ and $n_b = 6(n_c - 2)^2$. Ordering the points in the interior first, the local indexing of the n discretization points associated with Ω^τ is $I^\tau = [I_i^\tau I_b^\tau]$.

We seek to approximate the solution to (1.1) on Ω^τ using classical spectral collocation [26] as given by

$$(2.1) \quad \mathbf{A}_c^\tau := -\mathbf{D}_x^2 - \mathbf{D}_y^2 - \mathbf{D}_z^2 - \mathbf{C}^\tau$$

where \mathbf{C}^τ is the diagonal matrix with entries $\{\kappa^2(1 - b(\mathbf{x}_k))\}_{k=1}^n$.

To construct the operator for enforcing the impedance boundary condition, we first order the indices in I_b^τ according to which face they lie on. Specifically, $I_b^\tau =$

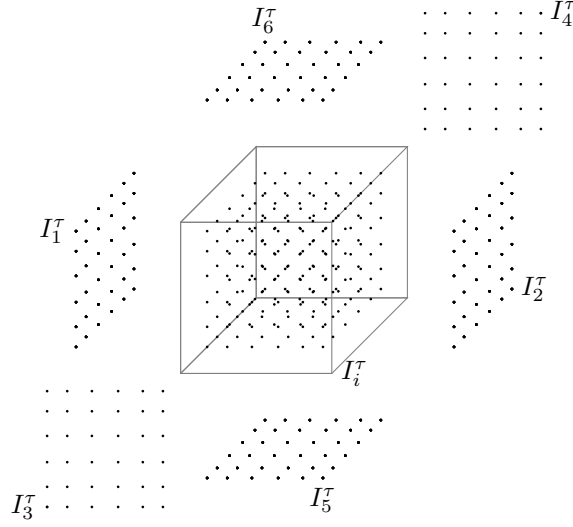


Fig. 2.1: Illustration of the the degree 8 Chebyshev tensor-product points on a cube Ω^τ and the local numbering of the nodes. I_i^τ denotes the interior nodes and I_j^τ for $j = 1, \dots, 6$ denotes the nodes on face j .

$[I_1^\tau, I_2^\tau, I_3^\tau, I_4^\tau, I_5^\tau, I_6^\tau]$ where I_1 denotes the index of the points on the left of the box, I_2 on the right, etc. Figure 2.1 illustrates the ordering for a box Ω^τ . To construct the approximation of the impedance boundary condition, we will utilize the derivative matrices. This means that the approximation of the derivative at the boundary can be constructed via the $n_b \times n$ matrix \mathbf{N} given by

$$(2.2) \quad \mathbf{N} = \begin{pmatrix} -\mathbf{D}_x(I_1^\tau, I^\tau) \\ \mathbf{D}_x(I_2^\tau, I^\tau) \\ -\mathbf{D}_y(I_3^\tau, I^\tau) \\ \mathbf{D}_y(I_4^\tau, I^\tau) \\ -\mathbf{D}_z(I_5^\tau, I^\tau) \\ \mathbf{D}_z(I_6^\tau, I^\tau) \end{pmatrix}.$$

Thus the impedance operator is approximated by the $n_b \times n$ matrix \mathbf{F}^τ defined by

$$\mathbf{F}^\tau = \mathbf{N} + i\eta \mathbf{I}_n(I_b^\tau, I^\tau),$$

where \mathbf{I}_n is the identity matrix of size $n \times n$.

Let \mathbf{u} denote the vector whose elements are the approximate solution on Ω^τ . The local linear system that results from this discretization of Ω^τ is

$$(2.3) \quad \mathbf{A}^\tau \begin{bmatrix} \mathbf{u}_i \\ \mathbf{u}_b \end{bmatrix} = \begin{bmatrix} \mathbf{A}_c^\tau(I_i^\tau, I^\tau) \\ \mathbf{F}^\tau \end{bmatrix} \begin{bmatrix} \mathbf{u}_i \\ \mathbf{u}_b \end{bmatrix} = \begin{bmatrix} \mathbf{s} \\ \hat{\mathbf{f}} \end{bmatrix}$$

where $\mathbf{u}_i = \mathbf{u}(I_i^\tau)$, $\mathbf{u}_b = \mathbf{u}(I_b^\tau)$, $\hat{\mathbf{f}}$ is fictitious impedance boundary data on $\partial\Omega^\tau$, and \mathbf{s} is the right hand side of the differential operator in (1.1) evaluated at the discretization points in the interior of Ω^τ .

2.2. Communication between leaf boxes. While the previous section provides a local discretization, it does not provide a way for the leaves (elements) to communicate information. The HPS method communicates information between elements by enforcing conditions on the continuity of the approximate solution and its flux through shared boundaries. For Helmholtz problems, this is done via continuity of impedance boundary data. In other words, the incoming impedance data for one element is equal to (less a sign) the outgoing impedance data from its neighbor along the shared face. Incoming and outgoing impedance boundary data and the relationship are defined as follows:

DEFINITION 2.2. Fix $\eta \in \mathbb{C}$, and $\Re(\eta) \neq 0$. Let

$$(2.4) \quad \begin{aligned} f &:= \frac{\partial u}{\partial n} + i\eta u|_{\Gamma}, \text{ and} \\ g &:= \frac{\partial u}{\partial n} - i\eta u|_{\Gamma} \end{aligned}$$

be Robin traces of u at an arbitrary interface Γ . $\frac{\partial u}{\partial n}$ denotes the normal derivative of u in the direction of the normal vector n . We refer to f and g as the incoming and outgoing (respectively) impedance data.

Let c_1 and c_2 be two neighboring subdomains, f_1 and g_2 the incoming and outgoing impedances at Γ respectively. We require

$$(2.5) \quad f_1 = -g_2$$

The operator approximating the outgoing impedance data on any leaf can be constructed via the same techniques presented in §2.1. Specifically, let \mathbf{N} be the Chebyshev differentiation matrix that approximates the flux as presented in equation (2.2). Then the outgoing impedance operator is

$$(2.6) \quad \mathbf{G}^\tau = \mathbf{N} - i\eta \mathbf{I}_n (I_b^\tau, I^\tau),$$

where \mathbf{I}_n is the $n \times n$ identity matrix, and η is an impedance parameter. In practice, we set $\eta = \kappa$.

In order to enforce this boundary condition, we replace the fictitious boundary data $\hat{\mathbf{f}}$ with the formula for negative outgoing impedance data from the neighboring leaf boxes.

3. The global system. The linear system that results from the discretization with N_ℓ leaves is

$$(3.1) \quad \mathbf{A}\mathbf{x} = \mathbf{b}$$

where \mathbf{A} is a $(N \times N)$ non-symmetric matrix, $N = nN_\ell$, with complex-valued entries and \mathbf{b} is the discretization of the right hand side for the interior nodes and zero for the leaf boundary nodes, since outgoing impedance operators are included as off-diagonal blocks of \mathbf{A} . The matrix \mathbf{A} is sparse. Figure 3.1(a) illustrates the block-sparsity pattern of the large system and Figure 3.1(b) illustrates a principal block-submatrix of this sparse system.

Remark 3.1. To keep computations local to each leaf, we allow each leaf box to have its own set of boundary nodes. This means that for all interior leaf boundary faces have twice as many unknowns as there are discretization points on that face.

$$(3.2) \quad \begin{aligned} \mathbf{G}_{-x}^\tau &:= \begin{pmatrix} \mathbf{0}^\tau(I_i^\tau, I^\tau) \\ \mathbf{G}^\tau(I_1^\tau, I^\tau) \\ \mathbf{0}^\tau(I_2^\tau, I^\tau) \\ \mathbf{0}^\tau(I_3^\tau, I^\tau) \\ \mathbf{0}^\tau(I_4^\tau, I^\tau) \\ \mathbf{0}^\tau(I_5^\tau, I^\tau) \\ \mathbf{0}^\tau(I_6^\tau, I^\tau) \end{pmatrix}, & \mathbf{G}_x^\tau &:= \begin{pmatrix} \mathbf{0}^\tau(I_i^\tau, I^\tau) \\ \mathbf{0}^\tau(I_1^\tau, I^\tau) \\ \mathbf{G}^\tau(I_2^\tau, I^\tau) \\ \mathbf{0}^\tau(I_3^\tau, I^\tau) \\ \mathbf{0}^\tau(I_4^\tau, I^\tau) \\ \mathbf{0}^\tau(I_5^\tau, I^\tau) \\ \mathbf{0}^\tau(I_6^\tau, I^\tau) \end{pmatrix}, & \mathbf{G}_{-y}^\tau &:= \begin{pmatrix} \mathbf{0}^\tau(I_i^\tau, I^\tau) \\ \mathbf{0}^\tau(I_1^\tau, I^\tau) \\ \mathbf{0}^\tau(I_2^\tau, I^\tau) \\ \mathbf{G}^\tau(I_3^\tau, I^\tau) \\ \mathbf{0}^\tau(I_4^\tau, I^\tau) \\ \mathbf{0}^\tau(I_5^\tau, I^\tau) \\ \mathbf{0}^\tau(I_6^\tau, I^\tau) \end{pmatrix}, \\ \mathbf{G}_y^\tau &:= \begin{pmatrix} \mathbf{0}^\tau(I_i^\tau, I^\tau) \\ \mathbf{0}^\tau(I_1^\tau, I^\tau) \\ \mathbf{0}^\tau(I_2^\tau, I^\tau) \\ \mathbf{0}^\tau(I_3^\tau, I^\tau) \\ \mathbf{G}^\tau(I_4^\tau, I^\tau) \\ \mathbf{0}^\tau(I_5^\tau, I^\tau) \\ \mathbf{0}^\tau(I_6^\tau, I^\tau) \end{pmatrix}, & \mathbf{G}_{-z}^\tau &:= \begin{pmatrix} \mathbf{0}^\tau(I_i^\tau, I^\tau) \\ \mathbf{0}^\tau(I_1^\tau, I^\tau) \\ \mathbf{0}^\tau(I_2^\tau, I^\tau) \\ \mathbf{0}^\tau(I_3^\tau, I^\tau) \\ \mathbf{0}^\tau(I_4^\tau, I^\tau) \\ \mathbf{G}^\tau(I_5^\tau, I^\tau) \\ \mathbf{0}^\tau(I_6^\tau, I^\tau) \end{pmatrix}, & \mathbf{G}_z^\tau &:= \begin{pmatrix} \mathbf{0}^\tau(I_i^\tau, I^\tau) \\ \mathbf{0}^\tau(I_1^\tau, I^\tau) \\ \mathbf{0}^\tau(I_2^\tau, I^\tau) \\ \mathbf{0}^\tau(I_3^\tau, I^\tau) \\ \mathbf{0}^\tau(I_4^\tau, I^\tau) \\ \mathbf{0}^\tau(I_5^\tau, I^\tau) \\ \mathbf{G}^\tau(I_6^\tau, I^\tau) \end{pmatrix}. \end{aligned}$$

where $\mathbf{0}$ denotes the zero matrix of size $n \times n$ and the non-zero matrices are submatrices of \mathbf{G}^τ as defined in equation (2.6). For example, consider an interior leaf τ (i.e. it does not share a boundary with the boundary of Ω). Then the matrices that are used to enforce the impedance conditions out of each boundary face are \mathbf{G}_{-x}^τ , \mathbf{G}_x^τ , \mathbf{G}_{-y}^τ , \mathbf{G}_y^τ , \mathbf{G}_{-z}^τ and \mathbf{G}_z^τ . Minus signs for outgoing impedance are used to enforce the continuity between neighboring boxes.

The solution technique presented in this paper utilizes an iterative solver such as GMRES. This means that it is necessary to apply the linear system that results from the discretization to a vector rapidly. Thanks to all the matrices being defined at the box (element) level, this is easily done in a *matrix-free* manner [16, 17]. Essentially for any block row, there are two matrices that need to be applied: the self interaction matrix corresponding to the discretization of the problem on a box as presented in §2.1 and the matrices that result from enforcing the continuity of the impedance boundary data between boxes. Fortunately these matrices are sparse. Figure 3.2 illustrates the sparsity pattern of some of these matrices when $n_c = 10$. Since the \mathbf{G}_x^τ , etc. matrices are very sparse (e.g. Figure 3.2(b)), their application to a vector is straightforward.

Of the matrices that need to be applied in a block row, the one corresponding to the discretization of the leaf box \mathbf{A}^τ is the largest. The most dense subblock is the principal $n_i \times n_i$ submatrix \mathbf{A}_{ii}^τ which corresponds to the differential operator on the interior nodes. The sparsity pattern of \mathbf{A}_{ii}^τ (illustrated in Figure 3.2(a)) results from the fact that the matrix is defined via Kronecker products. Specifically, the matrix \mathbf{A}_{ii}^τ is defined as follows

$$(3.3) \quad \mathbf{A}_{ii}^\tau = -\mathbf{I}_{(n_c-2)} \otimes \mathbf{I}_{(n_c-2)} \otimes \mathbf{L}_1 - \mathbf{I}_{(n_c-2)} \otimes \mathbf{L}_1 \otimes \mathbf{I}_{(n_c-2)} - \mathbf{L}_1 \otimes \mathbf{I}_{(n_c-2)} \otimes \mathbf{I}_{(n_c-2)} - \mathbf{C}_{ii}^\tau$$

where $\mathbf{I}_{(n_c-2)}$ denotes the $(n_c-2) \times (n_c-2)$ identity matrix, \mathbf{L}_1 denotes the $(n_c-2) \times (n_c-2)$ submatrix of the Chebyshev differentiation matrix used for approximating the second derivative of a one dimensional function, and \mathbf{C}_{ii}^τ denotes the operator \mathbf{C}^τ on the interior nodes. This tensor product structure allows for the matrix \mathbf{A}_{ii}^τ to be applied rapidly via the technique presented in Lemma 3.2 which was first presented in [21].

LEMMA 3.2. Let $\mathbf{x} = \text{vec}(\mathbf{X})$ denote the vectorization of the $m \times m$ matrix \mathbf{X} formed by stacking the columns of \mathbf{X} into a single column vector \mathbf{x} . Likewise, let \mathbf{y} denote the vectorization of the $m \times m$ matrix \mathbf{Y} . Let \mathbf{M} and \mathbf{N} denote matrices of

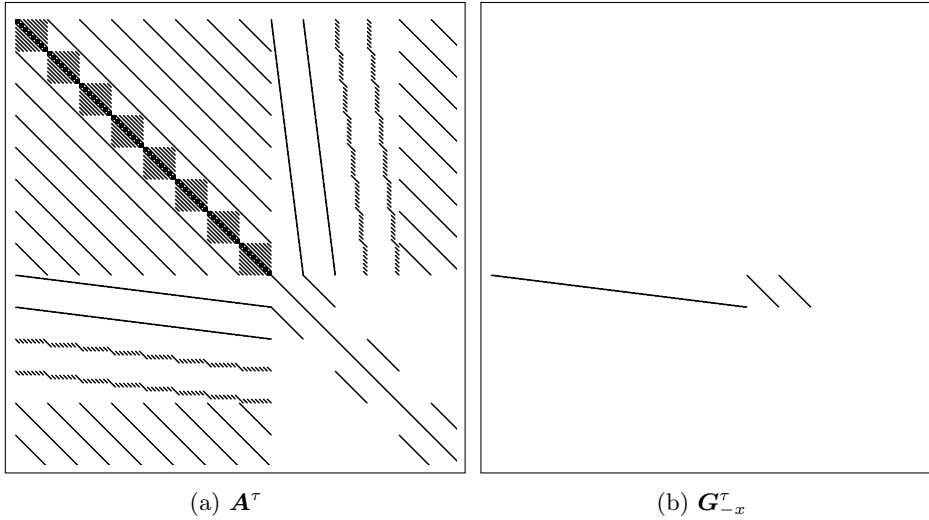


Fig. 3.2: Illustration of sparsity pattern of the matrices (a) \mathbf{A}^T and (b) \mathbf{G}_{-x}^T when the discretization technique is applied to leaf boxes with $n_c = 10$.

size $m \times m$. The Kronecker product matrix vector multiplication

$$\mathbf{y} = (\mathbf{M} \otimes \mathbf{N})\mathbf{x}$$

can be evaluated by creating the vectorization of the following

$$\mathbf{Y} = \mathbf{N}\mathbf{X}\mathbf{M}^T.$$

In other words, $\mathbf{y} = \text{vec}(\mathbf{N}\mathbf{X}\mathbf{M}^T)$.

Proof. See [21]. □

The technique in Lemma 3.2 is able to dramatically reduce the cost of applying \mathbf{A}_{ii}^T to a vector because the evaluation of the matrix-matrix products has a lower computational cost than building the large Kronecker product matrix and evaluating the matrix-vector multiplication after that. In the application of \mathbf{A}_{ii}^T additional acceleration is gained because in each set of Kronecker products two of the matrices involved are identity matrices. Algorithm 1 details the fast application of the matrix \mathbf{A}_{ii}^T . Algorithm 2 presents the efficient technique for evaluating the global matrix-vector multiplication.

4. The Preconditioner. While the sparse linear system that arises from the HPS discretization can be applied rapidly, its condition number is highly dependent on the condition number of the leaf discretization. It is for this reason that this paper presents an efficient block Jacobi preconditioner. In other words, the proposed solution technique is to use an iterative solver to find \mathbf{x} such that

$$(4.1) \quad \mathbf{J}^{-1}\mathbf{A}\mathbf{x} = \mathbf{J}^{-1}\mathbf{b}$$

where \mathbf{J} is the block Jacobi preconditioner. In order for this to be a viable solution technique, the matrix \mathbf{J}^{-1} must be efficient to construct and apply to a vector. The

ALGORITHM 1 (Fast application of \mathbf{A}_{ii}^τ)

Let \mathbf{v} be a vector of size n_i , the algorithm calculates $\mathbf{w} = \mathbf{A}_{ii}^\tau \mathbf{v}$. Let $n_1 := n_c - 2$. The function $\text{reshape}(\cdot, (p, q))$ is the classical reshape by columns function, as found in MATLAB and FORTRAN implementations.

-
- (1) $\mathbf{M}_1 = \text{reshape}(\mathbf{v}, (n_1^2, n_1))$
 - (2) $\mathbf{w}_1 = \text{vec}(\mathbf{M}_1 \mathbf{L}_1^\top)$
 - (3) **for** $j = 1, \dots, n_1$
 - (4) $\mathbf{M}_2(:, j) = \text{vec}(\text{reshape}(\mathbf{M}_1(:, j), (n_1, n_1)) \mathbf{L}_1^\top)$
 - (5) **end do**
 - (6) $\mathbf{w}_2 = \text{vec}(\mathbf{M}_2)$
 - (7) **for** $j = 1, \dots, n_1$
 - (8) $\mathbf{M}_2(:, j) = \text{vec}(\mathbf{L}_1 \text{reshape}(\mathbf{M}_1(:, j), (n_1, n_1)))$
 - (9) **end for**
 - (10) $\mathbf{w}_3 = \text{vec}(\mathbf{M}_2)$
 - (11) $\mathbf{w} = -\mathbf{w}_1 - \mathbf{w}_2 - \mathbf{w}_3 + \mathbf{C}_{ii}^\tau \mathbf{v}$

ALGORITHM 2 (Application of the forward operator \mathbf{A})

Let

$$\mathbf{v} = \begin{pmatrix} \mathbf{v}^{\tau=1} \\ \dots \\ \mathbf{v}^{\tau=N_\ell} \end{pmatrix}$$

be a vector of size N , where

$$\mathbf{v}^\tau = \begin{pmatrix} \mathbf{v}_i^\tau \\ \mathbf{v}_b^\tau \end{pmatrix}$$

is the sub-vector of size $n = n_i + n_b$ associated to leaf τ , where \mathbf{v}_i^τ is of size n_i and \mathbf{v}_b^τ is of size n_b . The vectors \mathbf{w} and \mathbf{w}^τ are defined in the same manner. The algorithm calculates $\mathbf{w} = \mathbf{A}\mathbf{v}$.

-
- (1) **for** $\tau = 1, \dots, N_\ell$
 - (2) calculate $\mathbf{w}_i^\tau = \mathbf{A}_{ii}^\tau \mathbf{v}_i^\tau + \mathbf{A}^\tau(I_i, I_b) \mathbf{v}_b^\tau$ using (3.3), Lemma 3.2 and sparse $\mathbf{A}^\tau(I_i, I_b)$,
 - (3) calculate $\mathbf{w}_b^\tau = \mathbf{F}(I_b, I_i) \mathbf{v}_i^\tau + \mathbf{F}(I_b, I_b) \mathbf{v}_b^\tau$ using sparse $\mathbf{F}(I_b, I_i)$ and $\mathbf{F}(I_b, I_b)$,
 - (4) **for** $j = -x, x, -y, y, -z, z$ **not on** $\partial\Omega$
 - (5) set $\mathbf{w}^\tau = \mathbf{w}^\tau + \mathbf{G}_j^\tau \mathbf{w}^\tau$, using definitions (3.2)
 - (6) **end for**
 - (7) **end for**

block Jacobi preconditioner is based on an efficient solver for the discretized leaf problems.

Recall that the local discretized problem (i.e. problem on a leaf) takes the form

$$\begin{bmatrix} \mathbf{A}_{ii}^\tau & \mathbf{A}_{ib}^\tau \\ \mathbf{F}_{bi}^\tau & \mathbf{F}_{bb}^\tau \end{bmatrix} \begin{bmatrix} \mathbf{u}_i^\tau \\ \mathbf{u}_b^\tau \end{bmatrix} = \begin{bmatrix} \mathbf{s}^\tau \\ \hat{\mathbf{f}}^\tau \end{bmatrix}.$$

Solving this system in 2×2 block form, we find that

$$(4.2) \quad \begin{aligned} \mathbf{u}_b^\tau &= \mathbf{S}^{\tau,-1} \left(\hat{\mathbf{f}}^\tau - \mathbf{F}_{bi}^\tau \mathbf{A}_{ii}^{\tau,-1} \mathbf{s}^\tau \right) \\ \mathbf{u}_i^\tau &= \mathbf{A}_{ii}^{\tau,-1} \left(\mathbf{s}^\tau - \mathbf{A}_{ib}^\tau \mathbf{u}_b^\tau \right) \end{aligned}$$

or in matrix form

$$(4.3) \quad \begin{bmatrix} \mathbf{u}_i^\tau \\ \mathbf{u}_b^\tau \end{bmatrix} = \begin{bmatrix} \mathbf{A}_{ii}^{\tau,-1} & -\mathbf{A}_{ii}^{\tau,-1} \mathbf{A}_{ib}^\tau \\ -\mathbf{S}^{\tau,-1} \mathbf{F}_{bi}^\tau \mathbf{A}_{ii}^{\tau,-1} & \mathbf{S}^{\tau,-1} \end{bmatrix} \begin{bmatrix} \mathbf{s}^\tau \\ \hat{\mathbf{f}}^\tau \end{bmatrix}$$

where

$$(4.4) \quad \mathbf{S}^\tau = \mathbf{F}_{bb}^\tau - \mathbf{F}_{bi}^\tau \mathbf{A}_{ii}^{\tau,-1} \mathbf{A}_{ib}^\tau$$

denotes the Schur complement matrix for leaf τ . Equations (4.2) are preferred to the matrix form since it allows the application of the inverse of the Schur complement once. If a low order discretization is used, then it is computationally viable to use the block inverse in (4.3) for the preconditioner. Since the HPS method uses high order discretizations, this is not a good option since the cost of building the inverse in (4.3) is dominated by inverting \mathbf{A}_{ii}^τ . While the matrix \mathbf{A}_{ii}^τ can be applied rapidly thanks to it being defined via a collection of Kronecker products plus a diagonal matrix, its inverse cannot be evaluated or applied efficiently when the scattering potential is not constant. Thus the technique in this paper uses an iterative solution technique based on local homogenization to build an exact block-Jacobi preconditioner. More specifically, the technique in this paper inverts \mathbf{A}_{ii}^τ *iteratively* using a GMRES solver which is preconditioned with the inverse of a homogenized version of \mathbf{A}_{ii}^τ . Let $\tilde{\mathbf{A}}_{ii}^\tau$ denote the matrix resulting from homogenization. Using the inverse of the homogenized operator as a preconditioner for \mathbf{A}_{ii}^τ is viable because it can be constructed via a tensor product structure (see §4.1) and leaf boxes are not many wavelengths in size. It is known that the homogenized operator is not a good preconditioner for high frequency problems since it is spectrally too different to its non-homogenized counterpart, unless restrictive assumptions like scale separation and periodicity of the medium are assumed for the variable coefficient [23].

A ‘‘homogenized’’ version of \mathbf{S}^τ , denoted $\tilde{\mathbf{S}}^\tau$, is generated by using $\tilde{\mathbf{A}}_{ii}^\tau$ in place of \mathbf{A}_{ii}^τ in (4.4). The application of the inverse of the true Schur complement \mathbf{S}^τ is created using GMRES preconditioned by $\tilde{\mathbf{S}}^\tau$. Section 4.2 provides details on this techniques.

Algorithm 5 details how these local preconditioners are put together to efficiently apply the true block-Jacobi preconditioner. Each application of the block-Jacobi preconditioner requires two nested iterative solves per leaf box.

Remark 4.1. The blocks of the Jacobi preconditioner presented in this section are built for each leaf independently. While this builds the best preconditioner of this form, it is possible to re-use the local preconditioners for multiple blocks (boxes). The effectiveness will depend on how much the function $b(\mathbf{x})$ varies over the geometry.

4.1. Homogenized preconditioner for inverting \mathbf{A}_{ii}^τ . This section presents a homogenized preconditioner for inverting the matrix \mathbf{A}_{ii}^τ . As stated in the introduction to this section, it is not computationally feasible to invert the matrix \mathbf{A}_{ii}^τ directly. This is because for variable coefficient Helmholtz problems, the diagonal entries of \mathbf{C}_{ii}^τ will not be constant. If the entries were constant, it would be possible to create a fast inversion method for \mathbf{A}_{ii}^τ . That is the inspiration for the preconditioner presented in this section.

Let λ^τ denote an average of the diagonal entries in the matrix \mathbf{C}_{ii}^τ . Specifically

$$\lambda^\tau = \frac{\max(\text{diag}(\mathbf{C}_{ii}^\tau)) + \min(\text{diag}(\mathbf{C}_{ii}^\tau))}{2}.$$

Then the homogenized discretized operator is

$$\tilde{\mathbf{A}}_{ii}^\tau = -\mathbf{I}_{(n_c-2)} \otimes \mathbf{I}_{(n_c-2)} \otimes \mathbf{L}_1 - \mathbf{I}_{(n_c-2)} \otimes \mathbf{L}_1 \otimes \mathbf{I}_{(n_c-2)} - \mathbf{L}_1 \otimes \mathbf{I}_{(n_c-2)} \otimes \mathbf{I}_{(n_c-2)} - \lambda \mathbf{I}_{n_i},$$

ALGORITHM 3 (Fast application of $\tilde{\mathbf{A}}_{ii}^{\tau,-1}$)

Let \mathbf{v} be a vector of size $n_i = n_1^3$ (where $n_1 = n_c - 2$), the algorithm calculates $\mathbf{w} = \tilde{\mathbf{A}}_{ii}^{\tau,-1} \mathbf{v}$.

The function $\text{reshape}(\cdot, (p, q))$ is the classical reshape by columns function, as found in MATLAB and FORTRAN implementations.

-
- (1) $\mathbf{M}_1 = \text{reshape}(\mathbf{v}, (n_1^2, n_1)) \tilde{\mathbf{V}}^{-1}$
 - (2) **for** $j = 1, \dots, n_1$
 - (3) $\mathbf{M}_2(:, j) = \text{vec}(\tilde{\mathbf{V}}^{-1} \text{reshape}(\mathbf{M}_1(:, j), (n_1, n_1)) (\tilde{\mathbf{V}}^{-1})^\top)$
 - (4) **end for**
 - (5) $\mathbf{M}_1 = \text{reshape}((\mathbf{E}_\Delta - \lambda \mathbf{I}_i)^{-1} \text{vec}(\mathbf{M}_2), (n_1^2, n_1)) \tilde{\mathbf{V}}$
 - (6) **for** $j = 1, \dots, n_1$
 - (7) $\mathbf{M}_2(:, j) = \text{vec}(\tilde{\mathbf{V}} \text{reshape}(\mathbf{M}_1(:, j), (n_1, n_1)) (\tilde{\mathbf{V}})^\top)$
 - (8) **end for**
 - (9) $\mathbf{w} = \text{vec}(\mathbf{M}_2)$
-

where \mathbf{I}_{n_i} is the inverse of size $n_i \times n_i$ and $\mathbf{I}_{(n_c-2)}$ is the $(n_c - 2) \times (n_c - 2)$ identity matrix. The inverse of this homogenized operator can be written down explicitly in terms of the eigenvalues and eigenvectors of the one-dimensional derivative matrix \mathbf{L}_1 .

Let $\mathbf{L}_1 = \mathbf{V} \mathbf{E} \mathbf{V}^{-1}$ denote the eigenvalue decomposition of the one dimensional derivative matrix \mathbf{L}_1 ; i.e. \mathbf{V} denotes the matrix whose columns are the eigenvectors of \mathbf{L}_1 and \mathbf{E} denotes the diagonal matrix with the non-zero entries being the corresponding eigenvalues. Then the three-dimensional discrete Laplacian can be written as

$$(4.5) \quad \mathbf{L}_3 = \tilde{\mathbf{V}} \mathbf{E}_\Delta \tilde{\mathbf{V}}^{-1}$$

where

$$\begin{aligned} \tilde{\mathbf{V}} &:= \mathbf{V} \otimes \mathbf{V} \otimes \mathbf{V}, \\ \mathbf{E}_\Delta &:= \mathbf{E} \otimes \mathbf{I}_{(n_c-2)} \otimes \mathbf{I}_{(n_c-2)} + \mathbf{I} \otimes \mathbf{E} \otimes \mathbf{I}_{(n_c-2)} \otimes \mathbf{I}_{(n_c-2)} + \mathbf{I}_{(n_c-2)} \otimes \mathbf{I}_{(n_c-2)} \otimes \mathbf{E} \text{ and} \\ \tilde{\mathbf{V}}^{-1} &:= \mathbf{V}^{-1} \otimes \mathbf{V}^{-1} \otimes \mathbf{V}^{-1}. \end{aligned}$$

Thus

$$\tilde{\mathbf{A}}_{ii}^\tau = \tilde{\mathbf{V}} (-\mathbf{E}_\Delta - \lambda \mathbf{I}_{n_i}) \tilde{\mathbf{V}}^{-1}$$

and its inverse is given by

$$\tilde{\mathbf{A}}_{ii}^{\tau,-1} = \tilde{\mathbf{V}} (-\mathbf{E}_\Delta - \lambda \mathbf{I}_{n_i})^{-1} \tilde{\mathbf{V}}^{-1}.$$

The inverse of $(-\mathbf{E}_\Delta - \lambda \mathbf{I}_{n_i})$ can be evaluated explicitly for little cost because \mathbf{E}_Δ consists of the Kronecker product of diagonal matrices. Additionally, $\tilde{\mathbf{A}}_{ii}^{\tau,-1}$ can be applied rapidly via the technique presented in Algorithm 3.

Now all instances of $\mathbf{A}_{ii}^{\tau,-1}$ in (4.2) can be replaced with a preconditioned GMRES solve. In other words, since the goal was to solve

$$(4.6) \quad \mathbf{A}_{ii}^\tau \mathbf{w} = \mathbf{v},$$

Table 4.1: MATLAB timings in seconds for solving (4.6) with $b(x) = 1.5e^{-160(x^2+y^2+z^2)}$ and $\kappa = 5$ using the Backslash command or the GMRES for the preconditioned problem (4.7) utilizing the fast sparse algebra for different discretization orders n_c . GMRES was run until there was a residual reduction of 10^{-8} . The error in the solution was compared against explicit inversion and is less than 10^{-7} for all experiments.

n_c	n	Backslash [s]	GMRES [s]
8	216	2.88E-03	2.86E-03
12	1000	2.20E-02	3.32E-03
16	2744	1.89E-01	4.04E-03
24	10648	3.51E+00	1.73E-02
32	27000	3.61E+01	2.73E-02

ALGORITHM 4

(Fast application of the Schur complement matrix $\mathbf{S} = \mathbf{F}_{bb}^\tau - \mathbf{F}_{bi}\mathbf{A}_{ii}^{-1}\mathbf{A}_{ib}$)
 Let \mathbf{v} be a vector of size n_b , the algorithm calculates the vector \mathbf{w} of size n_b defined as $\mathbf{w} = \mathbf{S}\mathbf{v}$.

- (1) $\tilde{\mathbf{v}}_1 = \mathbf{A}_{ib}^\tau \mathbf{v}$ where the sparsity of \mathbf{A}_{ib}^τ is exploited in the matvec.
- (2) Use GMRES to solve the homogenized preconditioned system
 $\tilde{\mathbf{A}}_{ii}^{\tau,-1} \mathbf{A}_{ii}^\tau \tilde{\mathbf{v}}_2 = \tilde{\mathbf{A}}_{ii}^{\tau,-1} \tilde{\mathbf{v}}_1$ as in §4.1
- (3) $\tilde{\mathbf{v}}_3 = \mathbf{F}_{bi}^\tau \tilde{\mathbf{v}}_2$ where \mathbf{F}_{bi} is applied exploiting sparsity.
- (4) $\mathbf{w} = \mathbf{F}_{bb}^\tau \mathbf{v} - \tilde{\mathbf{v}}_3$

the preconditioned linear system is

$$(4.7) \quad \tilde{\mathbf{A}}_{ii}^{\tau,-1} \mathbf{A}_{ii}^\tau \mathbf{w} = \tilde{\mathbf{A}}_{ii}^{\tau,-1} \mathbf{v}.$$

Table 4.1 compares the time in seconds it takes to solve (4.6) via the backslash operator in MATLAB with solving (4.7) via GMRES utilizing the fast matrix vector multiplication routines (implemented also in MATLAB) for different order discretizations. This experiment starts with $n_c = 8$ since this is when the number of interior nodes n_i is the same as the number of boundary nodes n_b . The results from the table show that the higher the order the greater the speed up from using the iterative solver. In practice, $n_c = 16$ is often used. For this experiment, the iterative solve is 47 times faster than using the backslash operator.

4.2. Homogenized preconditioner for inverting the Schur complement.

The inverse of the Schur complement matrix \mathbf{S}^τ is needed in the block solve of the locally discretized problem; see equation (4.3). While the technique in the previous section is efficient for inverting \mathbf{A}_{ii}^τ , it does not resolve all the efficiency problems in the block solve. This is because the Schur complement matrix is dense and moderate in size for high order discretizations. For example, when $n_c = 16$, the Schur complement is a matrix of size 1176×1176 . Thus we choose to use an iterative solver for applying the inverse of \mathbf{S}^τ instead of constructing it directly.

To get the iterative solver to converge rapidly, the linear system involving \mathbf{S}^τ is preconditioned by a homogenized Schur complement $\tilde{\mathbf{S}}^{\tau,-1}$. The proposed homoge-

ALGORITHM 5 (Application of the block-Jacobi preconditioner \mathbf{J}^{-1})

Let

$$\mathbf{v} = \begin{pmatrix} \mathbf{v}^{\tau=1} \\ \vdots \\ \mathbf{v}^{\tau=N^\tau} \end{pmatrix}$$

be a vector of size $N^\tau n^\tau$, where

$$\mathbf{v}^\tau = \begin{pmatrix} \mathbf{v}_i^\tau \\ \mathbf{v}_b^\tau \end{pmatrix}$$

is the sub-vector associated to leaf τ (respectively $\mathbf{w}, \mathbf{w}^\tau$). The algorithm calculates $\mathbf{w} = \mathbf{J}^{-1}\mathbf{v}$.

-
- (1) **for** $\tau = 1, \dots, N_\ell$
 - (2) calculate $\mathbf{f}_i = \mathbf{A}_{ii}^{\tau,-1}\mathbf{v}_i$ using §4.1,
 - (3) calculate $\mathbf{h}_b = \mathbf{A}_{bi}^\tau \mathbf{f}_i - \mathbf{v}_b$ using a sparse \mathbf{A}_{bi}^τ ,
 - (4) use GMRES to solve $\tilde{\mathbf{S}}^{\tau,-1} \mathbf{S}^\tau \mathbf{g}_b = \tilde{\mathbf{S}}^{\tau,-1} \mathbf{h}_b$ as in §4.2,
 - (5) $\mathbf{w}^\tau = \begin{pmatrix} \mathbf{f}_i + \mathbf{A}_{ii}^{\tau,-1} \mathbf{A}_{ib}^\tau \mathbf{g}_b \\ \mathbf{g}_b \end{pmatrix}$ using §4.1 and sparse \mathbf{A}_{ib}^τ .
 - (6) **end for**
-

nized Schur complement is defined by

$$\tilde{\mathbf{S}}^\tau = \mathbf{F}_{bb}^\tau - \mathbf{F}_{bi}^\tau \tilde{\mathbf{A}}_{ii}^{\tau,-1} \mathbf{A}_{ib}^\tau.$$

This is inexpensive to construct since $\tilde{\mathbf{A}}_{ii}^{\tau,-1}$ is already constructed for the preconditioner of \mathbf{A}_{ii}^τ . The matrix $\tilde{\mathbf{S}}^\tau$ is dense but since n_b is never too large compared to n_i , $\tilde{\mathbf{S}}^\tau$ can be inverted rapidly using standard linear algebra packages (e.g. LAPACK) and stored.

Now $\mathbf{S}^{\tau,-1}$ in (4.2) can be replaced with a preconditioned GMRES solve. In other words, since the goal was to solve

$$(4.8) \quad \mathbf{S}^\tau \mathbf{w} = \mathbf{v},$$

the preconditioned linear system is

$$(4.9) \quad \tilde{\mathbf{S}}^{\tau,-1} \mathbf{S}^\tau \mathbf{w} = \tilde{\mathbf{S}}^{\tau,-1} \mathbf{v}.$$

4.3. The block-Jacobi preconditioner. Finally, all the ingredients from the earlier sections can be put together to construct the block-Jacobi preconditioner. Algorithm 5 presents the application of the preconditioner for the full linear system. In all, solving the full linear system (4.1) with the complete algorithm requires three nested GMRES iterative solvers.

5. Implementation. This section describes the implementation of the method developed above, including hardware, compilers, libraries and related software. The code used for the numerical experiments in Section 6 is written in FORTRAN 90.

5.1. Algebraic operations and sparse matrices. The inversion of matrices, eigenvalue calculations, sparse and full matrix-matrix and matrix-vector operations using complex types are performed using the Intel MKL library. The codes are compiled using Intel FORTRAN compilers and libraries version 20.2. We use the MKL CSR format and the associated routines for algebraic operations with sparse matrices. Leaf matrices are never constructed explicitly. The largest matrices that are constructed are

the homogenized Schur complement preconditioners; $\tilde{\mathbf{S}}^{\tau,-1}, \forall \tau$; which are relatively small in size ($n_b \times n_b$).

5.2. Distributed memory. The parallelization and global solvers are accessed through the PETSC library version 3.8.0. We use the KSP implementation of GMRES present in PETSC and the `MatCreateShell` interface for the matrix-free algorithms representing \mathbf{A} and \mathbf{J}^{-1} . The message-passing implementation between computing nodes uses Intel MPI version 2017.0.098.

5.3. Hardware. All experiments in Section 6, were run on the RMACC Summit supercomputer. The system has peak performance of over 400 TFLOPS. The 472 general compute nodes each have 24 cores aboard Intel Haswell CPUs, 128 GB of RAM and a local SSD.

All nodes are connected through a high-performance network based on Intel Omni-Path with a bandwidth of 100 GB/s and a latency of 0.4 microseconds. A 1.2 PB high-performance IBM GPFS file system is provided.

6. Numerical results. This section illustrates the performance of the solution technique presented in this paper. In all the experiments, the domain Ω is the unit cube $[0, 1]^3$ and the variable coefficient function in (1.1) is defined as

$$(6.1) \quad b(\mathbf{x}) = -1.5e^{-160((x-0.5)^2+(y-0.5)^2+(z-0.5)^2)},$$

representing a Gaussian *bump* centered in the middle of the unit cube. The Chebyshev polynomial degree is fixed with $n_c = 16$. This follows the two dimensional discretization versus accuracy study in [7, §4.1]. Also, this choice of discretization order falls into the regime where the local preconditioner was shown to be effective in Section 4.1. The GMRES solver stops when the preconditioned residual reduction meets a specified criteria. The preconditioned residual at iteration k is $r_k = \|\mathbf{J}^{-1}(\mathbf{b} - \mathbf{A}\mathbf{x}_k)\|_2$ where \mathbf{x}_k is the approximate solution at iteration k .

Section 6.1 illustrates the strong and weak scaling of the solver. Since the accuracy of the solution technique is dictated by the discretization and not the stopping criteria for GMRES, it is important to have an idea of what to set the stopping criteria to so that all the digits attainable by the discretization are achieved. The stopping criteria so that all the possible digits attainable by the discretization are realized is called the *Reference Preconditioned Residual Reduction* (RPRR). Any extra iterations do not contribute the accuracy of the approximation and are expensive, so there should be as few of them as possible. A rule relating to RPRR to the accuracy of the discretization is found for a separable solution (which is easily represented by the local tensor product basis) in Section 6.2. Then the rule is applied to a non-separable problem and its performance is assessed in Section 6.3. In these experiments, the known solutions are used to generate the source and boundary data.

The relative error used in the experiments in Sections 6.2 and 6.3 is defined by

$$(6.2) \quad E_h = \frac{\sqrt{\sum_{i=1}^N (u_h(\mathbf{x}_i) - u(\mathbf{x}_i))^2}}{\sqrt{\sum_{i=1}^N u(\mathbf{x}_i)^2}},$$

where $N = N_\ell n$ is the total number of unknowns, $u_h(\mathbf{x})$ is the approximate solution at the point \mathbf{x} obtained by allowing GMRES to run until the residual reduction reaches

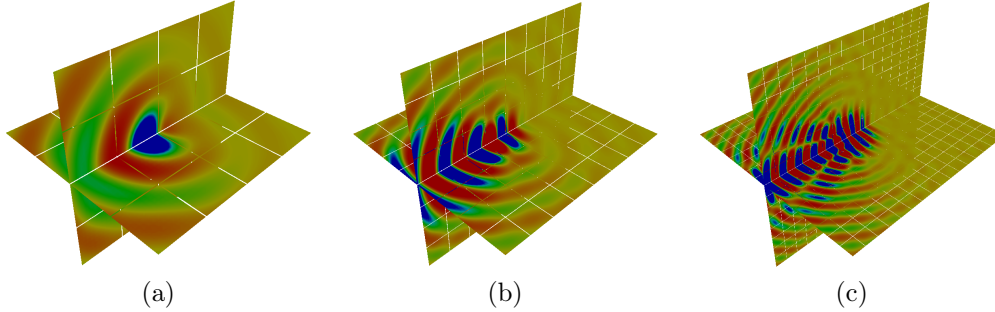


Fig. 6.1: Illustration of the exact solution on the planes $y = 0.5$ and $z = 0.5$ for a problem with (a) $\kappa = 20$ and 4^3 leaves, (b) $\kappa = 40$ and 8^3 leaves, and (c) $\kappa = 80$ and 16^3 leaves from left to right. The x -axis runs diagonally to the right, the y -axis diagonally to the left and the z -axis is vertical.

machine precision, $u(\mathbf{x})$ is the evaluation of the exact solution at the point \mathbf{x} , and N_ℓ is the number of leaf boxes. The superscript “it” denotes the approximation error obtained by the iterative solver with a specified stopping criteria; i.e. E_h^{it} is the error of the approximation $u_h^{\text{it}}(\mathbf{x}_i)$.

6.1. Scaling. This section investigates the scaling of the parallel implementation of the solver and the solution technique’s ability to address large problems using distributed memory. To assess performance, data is collected to draw strong and weak scaling curves. The strong scaling timings are for the same problem while increasing the number of processors. The weak scaling timings are generated by increasing the number of processors utilized while keeping the problem size per processor fixed.

Both for strong and weak scaling, we set $s(\mathbf{x}) = b(\mathbf{x})e^{i\kappa\mathbf{x}}$. Figure 6.1 illustrates the solution plotted on the planes $y = 0.5$ and $z = 0.5$ for $\kappa = 20, 40$, and 80 with $4^3, 8^3$, and 16^3 leaves, respectively.

6.1.1. Strong scaling. For the strong scaling experiment, the solution time versus the number of processors for a fixed problem size is considered, using a fixed preconditioned residual reduction of 10^{-8} . We consider the problem presented in the beginning of the section with $\kappa = 40$ and 8^3 leaf boxes (see Figure 6.1(b)). The number of MPI processes gets doubled in each experiment and results in a reduction of time. Figure 6.2 reports the scaling results. The run times reduce from approximately 20 minutes for a sequential execution to only a few minutes for a 32 MPI processor parallelization. The 32 MPI processor case only has 2 leaves per processor, which implies that there is lots of inter-process communication in that experiment. Even so, the run time is significantly shorter than the 16 processor case. This is because the algorithm performs the bulk of calculations locally given the high Chebyshev polynomial order. For all other cases, the run time approximately halves when the amount of processors is doubled which is expected from a well implemented distributed memory model.

6.1.2. Weak scaling. Weak scaling investigates how the solution time varies with the number of processors for a fixed problem size per processor and a fixed residual reduction. The discretization is refined and at the same time more MPI processes are used in order to keep the number of degrees of freedom per processor

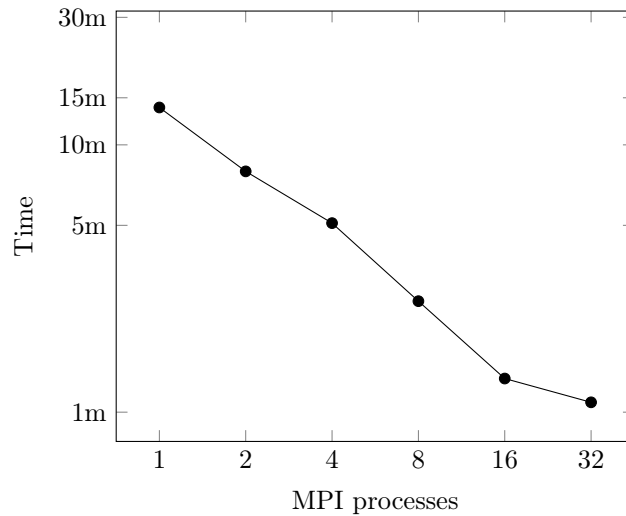


Fig. 6.2: Strong scaling: The time in minutes versus the number of MPI processor when applying the presented solution technique to a problem discretized with 8^3 leaf boxes.

constant. Two experiments are considered for weak scaling: a fixed wave number for all experiments and an increased wave number which maintains a fixed number of points per wavelength (ppw) while the mesh is refined. The latter is representative of the types of experiments solved by practitioners.

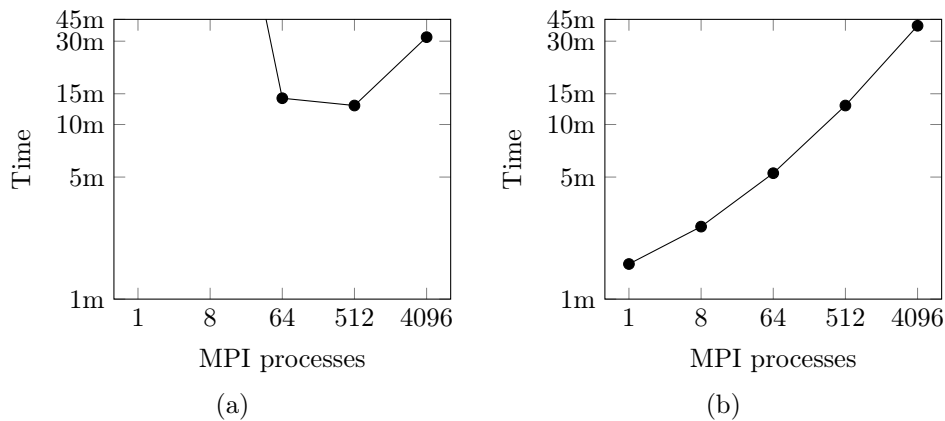


Fig. 6.3: Weak scaling: Time in minutes for solving (a) fixed wave number problem with $\kappa = 160$ and (b) maintaining 16 ppw on a geometry with a fixed $4 \times 4 \times 4$ leaves local problem on each processor.

Figure 6.3 reports the weak scaling for when the local problem size is fixed to 4^3 ; i.e. 4^3 leaf boxes are assigned to each processor and the residual reduction is fixed at 10^{-8} .

Problem size in leaves	$4 \times 4 \times 4$	$8 \times 8 \times 8$	$16 \times 16 \times 16$	$32 \times 32 \times 32$	$64 \times 64 \times 64$
MPI procs	1	8	64	512	4096
Degrees of freedom N	250k	2M	16M	128M	1027M
GMRES iterations	87	158	298	570	1114
GMRES time	95s	156s	316s	645s	2206s
Peak memory per process	2.47 GB	3.20 GB	3.42 GB	3.60 GB	3.70 GB

Table 6.1: MPI processors (MPI procs), number of discretization points, number of GMRES iterations, time for the iterative solver to converge with a preconditioned relative residual of 10^{-8} , and the peak memory per processor for different problem sizes. Here the wave number is increased to maintain 16 ppw.

Figure 6.3(a) reports on the performance when the wave number fixed to $\kappa = 160$. The problems range from 5 to half a wavelength per leaf. The experiments corresponding to a small number of processors have many wavelengths per leaf. This is a situation where it is well-known that local homogenization will not work well [10] and the increased timings are an expected result. As the number of wavelengths per leaf decreases so that the local problems are closer to elliptic, the homogenized preconditioner performs well and the performance of the global solver is significantly better.

Figure 6.3(b) reports on the weak scaling performance for experiments where the wave number is increased to maintain 16 ppw. The run times grow roughly linearly as the number of processors is increased. The shape of the curve is roughly linear at high frequencies, when the homogenized preconditioners work best. This means that the locally defined preconditioner is doing a good job killing the highly oscillatory residual components that tend to propagate through the geometry during the iterative solution process. This behavior is expected of a block-Jacobi preconditioner. From non-overlapping Schwarz domain decomposition theory, it is known that the runtime growth constant is proportional to the maximum distance between opposite sides of the domain, counted in leaves sharing a side.

The largest problem under consideration, corresponding to the 4096 MPI processor experiment in Figure 6.1(b), is approximately $50 \times 50 \times 50$ wavelengths in size and requires over a billion discretization points to achieve the set accuracy. Using the solver presented in this manuscript, this large problem is able to be solved in under 45 minutes.

Table 6.1 reports the scaling performance including the memory usage. Since the increase in memory per processor is low as the problem grows, it is possible to solve large problems on the **RMACC Summit** cluster nodes which have 4.6 GB per node. In fact, the memory per processor is under 4 GB for all the experiments. This is because the method exploits the Kronecker product structure and the sparsity of operators.

6.2. Relative residual rule for maximum accuracy. This section considers the performance of the boundary value problem with an exact solution of

$$(6.3) \quad u(x, y, z) = e^{i\kappa(x+y+z)} e^x \cosh(y)(z+1)^2$$

with different wave numbers κ and a variable coefficient $b(\mathbf{x})$ defined in equation (6.1). Figure 6.4 illustrates the solution for different values of κ and that it is a plane wave in the direction $(1, 1, 1)$ that is modulated differently along the x , y and z axes. These experiments investigate how the stopping criteria of the iterative solver relates to the accuracy of the solution with the specified discretization.

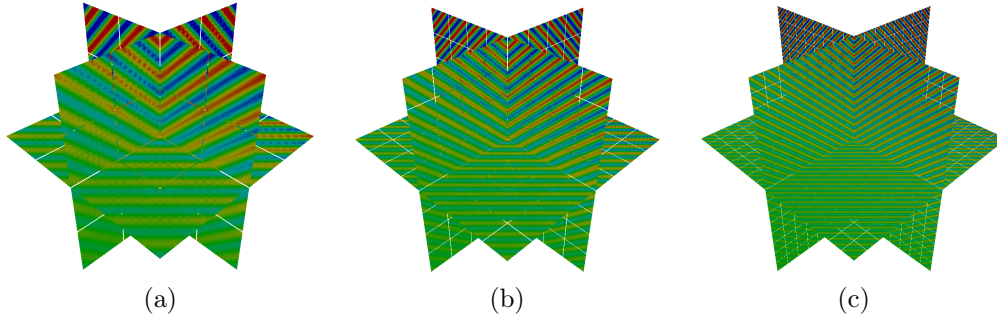


Fig. 6.4: Illustration of the exact solution (6.3) when 9.6 ppw is maintained for 4^3 , 8^3 and 16^3 leaves (from left to right). The plots of the solution are on the planes $x = 0.5$, $y = 0.5$ and $z = 0.5$ where the x -axis runs diagonally to the right, the y -axis diagonally to the left and the z -axis is vertical.

Table 6.2: Plane wave: The relative error E_h and number of digits of accuracy obtained for different ppw and number of leaf boxes.

Leaves \ ppw	4^3	8^3	16^3	32^3	Digits
24.0	2.057E-12	1.763E-12	1.715E-12	1.727E-12	11
19.2	8.872E-11	9.166E-11	9.275E-11	9.360E-11	10
16.0	1.514E-09	1.922E-09	1.631E-09	1.667E-09	8
12.0	7.121E-08	7.246E-08	7.221E-08	7.313E-08	7
9.60	6.932E-07	5.631E-07	4.836E-07	4.478E-07	6

Table 6.2 reports the relative error E_h and digits of accuracy obtained by the discretization when the number of ppw remains fixed across a row. Since the linear systems are too large to invert directly, the approximate solution u_h used to calculate E_h is obtained by iterating GMRES until the relative error E_h^{it} has converged. The error E_h related to the ppw remains fixed as expected by the two dimensional results. The values range from orders of magnitude of 10^{-12} for 24 ppw to 10^{-7} for 9.6 ppw. This accuracy matches the expected results based on the existing two dimensional work.

Remark 6.1. The ppw are measured by counting the points along the axes. For the plane wave problem, there are three times more points per wavelength along the diagonal of the box defined by the line $(1, 1, 1)$ along any axis.

Table 6.3 reports the RPRR which was defined at the beginning of §6. This table is generated by determining E_h^{it} at each iteration and stops when the digits of accuracy from Table 6.2 are obtained. The last column shows a safe convergence criteria for the preconditioned residual reduction such that E_h and E_h^{it} are negligibly different, i.e. the RPRR. Table 6.4 reports the corresponding times and number of iterations needed to obtain the residual reduction in Table 6.3. The results in the tables suggest that it is sufficient to ask for the residual reduction to be about two digits more than the expected accuracy of the discretization.

Table 6.4 shows that the solution technique takes longer as the number of points per wavelength decreases. This is expected because as the number of points per

Table 6.3: Plane wave: preconditioned residual reduction needed to achieve the maximum digits shown in Table 6.2 and choice of RPRR to ensure the maximum digits.

Leaves		4 ³	8 ³	16 ³	32 ³	RPRR
ppw						
	24.0	8.122E-13	1.632E-12	8.844E-13	5.231E-13	10 ⁻¹³
	19.2	8.883E-12	6.632E-12	3.534E-12	1.917E-12	10 ⁻¹²
	16.0	1.275E-09	1.681E-09	1.021E-09	5.151E-10	10 ⁻¹⁰
	12.0	1.438E-08	1.145E-08	7.215E-09	3.326E-09	10 ⁻⁹
	9.60	2.541E-07	1.385E-07	8.280E-08	4.408E-08	10 ⁻⁸

Table 6.4: Plane wave: GMRES time and number of iterations needed to achieve E_h for each choice of ppw and discretization.

Leaves		4 ³		8 ³		16 ³		32 ³	
ppw		time[s]	its.	time[s]	its.	time[s]	its.	time[s]	its.
	24.0	203	216	317	294	577	474	1298	772
	19.2	275	183	269	265	575	393	979	668
	16.0	280	141	230	178	411	272	726	465
	12.0	595	122	389	153	491	233	912	402
	9.6	2764	109	1297	138	824	190	1047	316

wavelength increases the leaf boxes become less elliptic and the local solves take longer to converge. In Table 6.4 looking left-to-right, the number of iterations and time to convergence increases. This is due to the global problem becoming larger in number of wavelengths as the number of leaf boxes increases.

6.3. Effectiveness of the proposed rule for stopping criteria. This section uses the proposed GMRES stopping criteria generated in the previous section. That is, the desired residual reduction is set to 2-3 digits more than the accuracy that can be achieved by the discretization.

The experiments in this section have an exact solution given by

$$(6.4) \quad u(x, y, z) = (1 + e^{i\kappa x}) (1 + e^{i\kappa y}) (1 + e^{i\kappa z}) \ln(1 + x^2 + y^2 + z^2)$$

which is not separable, and a variable coefficient $b(\mathbf{x})$ defined in equation (6.1). Figure 6.5 illustrates the solution (6.4) for different values of κ . Roughly speaking, it is a grid of bumps along any axis that is modulated by the function $\ln(1 + x^2 + y^2 + z^2)$. The pattern of bumps makes it easy to observe the number of wavelengths along the axes. Given that this solution is more oscillatory (with roughly the same magnitude) throughout the geometry than the solution in the previous section, it is expected that it will take more iterations for GMRES to converge. This is especially true for high frequency problems.

Table 6.5 reports the relative error E_h^{it} obtained by using the relative residual stopping criteria prescribed in the Section 6.2. The orders of magnitude in the error are similar to what was observed for the separable solution in Table 6.2 confirming the accuracy of the discretization. Table 6.6 reports the maximum achievable accuracy of the discretization E_h . The two errors are of the same order. This means that the stopping criteria is giving the maximum possible accuracy attainable by the

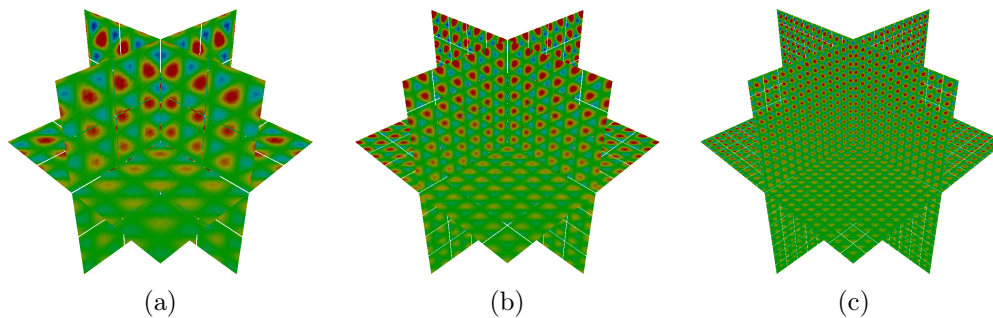


Fig. 6.5: Illustration of the *bumps* solution (6.4) cut at the planes $x = 0.5$, $y = 0.5$ and $z = 0.5$ for 9.6 ppw with discretizations consisting of (a) 4^3 , (b) 8^3 and (c) 16^3 leaves. The x -axis runs diagonally to the right, the y -axis diagonally to the left and the z -axis is vertical.

Table 6.5: Bumps: E_h^{it} and digits of accuracy obtained for different ppw and discretizations using the RPRR rule, showing that all the digits expected are effectively obtained.

ppw \ Leaves	4^3	8^3	16^3	32^3
24.0	3.647E-12	3.957E-12	6.770E-12	1.270E-11
19.2	1.456E-10	2.933E-10	5.432E-10	1.004E-09
16.0	2.930E-09	7.184E-09	1.377E-08	2.869E-08
12.0	1.528E-07	2.629E-07	4.573E-07	7.196E-07
9.60	5.389E-06	1.614E-06	2.857E-06	4.461E-06

discretization.

Table 6.7 reports the times and number of iterations needed for GMRES to converge with the prescribed residual reduction. As expected, more iterations are needed to solve these problems than in the experiments in Section 6.2 even though the discretizations achieve the same accuracy.

7. Concluding remarks. This manuscript presented an efficient iterative solution technique for the linear system that results from the HPS discretization of variable coefficient Helmholtz problems. The technique is based on a block-Jacobi preconditioner coupled with GMRES. The application of the preconditioner utilizes two local iterative solves on the leaf but all matrices can be applied rapidly thanks to their sparsity and Kronecker product structure.

The numerical results illustrate the effectiveness of the solution technique. While the method does not “scale” in the parallel computing context, it is extremely efficient. For example, it is able to solve a three dimensional mid frequency Helmholtz problem requiring over 1 billion discretization points to achieve 7 digits of accuracy in under 45 minutes on a cluster. The numerical results also illustrated that the HPS method is able to achieve a prescribed accuracy at set ppw. This is consistent with the accuracy observed for two dimensional problem [7, 13]. Additionally, the numerical results indicate that it is sufficient to ask for the relative residual of approximately 2-3 digits

Table 6.6: Bumps: E_h obtained for different ppw and discretizations

ppw \ Leaves	Leaves			
	4^3	8^3	16^3	32^3
24.0	3.738E-12	3.856E-12	6.736E-12	1.263E-11
19.2	1.480E-10	3.035E-10	5.432E-10	1.004E-09
16.0	2.910E-09	6.588E-09	1.376E-08	2.861E-08
12.0	1.528E-07	2.630E-07	4.573E-07	7.197E-07
9.60	1.302E-06	1.614E-06	2.856E-06	4.458E-06

Table 6.7: Bumps: GMRES time and iterations to achieve maximum accuracy using the RPRR rule.

ppw \ Leaves	4^3		8^3		16^3		32^3	
	time[s]	its.	time[s]	its.	time[s]	its.	time[s]	its.
24.0	219	247	292	346	657	559	1168	931
19.2	284	215	347	289	533	452	1722	829
16.0	290	163	287	224	448	371	978	691
12.0	736	144	561	182	564	308	1323	567
9.6	2083	96	1618	172	1015	264	1471	469

more than the accuracy expected of the discretization. This will minimize the number of extra iterations performed by GMRES.

As mentioned in the text, the proposed solver does not scale. In future work, the authors will develop a multi-level solver where the block-Jacobi preconditioner will be used as smoother between the coarse and the fine grids. Efficient solvers for the coarse grid is ongoing work.

Acknowledgements. The authors wish to thank Total Energies for their permission to publish. The work by A. Gillman is supported by the National Science Foundation (DMS-2110886). A. Gillman, J.P. Lucero Lorca and N. Beams are supported in part by a grant from Total Energies.

REFERENCES

- [1] I. BABUŠKA, F. IHLENBURG, E. T. PAIK, AND S. A. SAUTER, *A generalized finite element method for solving the Helmholtz equation in two dimensions with minimal pollution*, Computer Methods in Applied Mechanics and Engineering, 128 (1995), pp. 325–359, [https://doi.org/https://doi.org/10.1016/0045-7825\(95\)00890-X](https://doi.org/https://doi.org/10.1016/0045-7825(95)00890-X).
- [2] I. M. BABUŠKA AND S. A. SAUTER, *Is the pollution effect of the fem avoidable for the Helmholtz equation considering high wave numbers?*, SIAM Journal on Numerical Analysis, 34 (1997), pp. 2392–2423, <https://doi.org/10.1137/S0036142994269186>, <https://doi.org/10.1137/S0036142994269186>, <https://arxiv.org/abs/https://doi.org/10.1137/S0036142994269186>.
- [3] S. BALAY, S. ABHYANKAR, M. F. ADAMS, J. BROWN, P. BRUNE, K. BUSCHELMAN, L. DALCIN, A. DENER, V. EIJKHOUT, W. D. GROPP, D. KARPEYEV, D. KAUSHIK, M. G. KNEPLEY, D. A. MAY, L. C. MCINNES, R. T. MILLS, T. MUNSON, K. RUPP, P. SANAN, B. F. SMITH, S. ZAMPINI, H. ZHANG, AND H. ZHANG, *PETSc Web page*. <https://www.mcs.anl.gov/petsc>, 2021, <https://www.mcs.anl.gov/petsc>.
- [4] S. BALAY, S. ABHYANKAR, M. F. ADAMS, J. BROWN, P. BRUNE, K. BUSCHELMAN, L. DALCIN, A. DENER, V. EIJKHOUT, W. D. GROPP, D. KARPEYEV, D. KAUSHIK,

- M. G. KNEPLEY, D. A. MAY, L. C. MCINNES, R. T. MILLS, T. MUNSON, K. RUPP, P. SANAN, B. F. SMITH, S. ZAMPINI, H. ZHANG, AND H. ZHANG, *PETSc users manual*, Tech. Report ANL-95/11 - Revision 3.15, Argonne National Laboratory, 2021, <https://www.mcs.anl.gov/petsc>.
- [5] S. BALAY, W. D. GROPP, L. C. MCINNES, AND B. F. SMITH, *Efficient management of parallelism in object oriented numerical software libraries*, in *Modern Software Tools in Scientific Computing*, E. Arge, A. M. Bruaset, and H. P. Langtangen, eds., Birkhäuser Press, 1997, pp. 163–202.
- [6] A. BAYLISS, C. GOLDSTEIN, AND E. TURKEL, *On accuracy conditions for the numerical computation of waves*, *Journal of Computational Physics*, 59 (1985), pp. 396–404, [https://doi.org/https://doi.org/10.1016/0021-9991\(85\)90119-6](https://doi.org/https://doi.org/10.1016/0021-9991(85)90119-6), <https://www.sciencedirect.com/science/article/pii/0021999185901196>.
- [7] N. N. BEAMS, A. GILLMAN, AND R. J. HEWETT, *A parallel shared-memory implementation of a high-order accurate solution technique for variable coefficient Helmholtz problems*, *Computers & Mathematics with Applications*, 79 (2020), pp. 996–1011, <https://doi.org/https://doi.org/10.1016/j.camwa.2019.08.019>, <https://www.sciencedirect.com/science/article/pii/S089812211930416X>.
- [8] T. BECK, Y. CANZANI, AND J. L. MARZUOLA, *Quantitative bounds on impedance-to-impedance operators with applications to fast direct solvers for PDEs*, 2021, <https://arxiv.org/abs/2103.14700>.
- [9] J. BOYD, *Chebyshev and Fourier Spectral Methods*, Dover, Mineola, New York, 2nd ed., 2001.
- [10] T. CHAUMONT FRELET, *Finite element approximation of Helmholtz problems with application to seismic wave propagation*, theses, INSA de Rouen, Dec 2015, <https://tel.archives-ouvertes.fr/tel-01246244>.
- [11] P. GELDERMANS AND A. GILLMAN, *An adaptive high order direct solution technique for elliptic boundary value problems*, *SIAM Journal on Scientific Computing*, 41 (2019), pp. A292–A315, <https://doi.org/10.1137/17M1156320>, <https://doi.org/10.1137/17M1156320>, <https://arxiv.org/abs/https://doi.org/10.1137/17M1156320>.
- [12] A. GEORGE, *Nested dissection of a regular finite element mesh*, *SIAM Journal on Numerical Analysis*, 10 (1973), pp. 345–363, <https://doi.org/10.1137/0710032>, <https://doi.org/10.1137/0710032>, <https://arxiv.org/abs/https://doi.org/10.1137/0710032>.
- [13] A. GILLMAN, A. H. BARNETT, AND P.-G. MARTINSSON, *A spectrally accurate direct solution technique for frequency-domain scattering problems with variable media*, *BIT Numerical Mathematics*, 55 (2015), pp. 141–170.
- [14] A. GILLMAN AND P. G. MARTINSSON, *A direct solver with $\mathcal{O}(n)$ complexity for variable coefficient elliptic PDEs discretized via a high-order composite spectral collocation method*, *SIAM Journal on Scientific Computing*, 36 (2014), pp. A2023–A2046, <https://doi.org/10.1137/130918988>.
- [15] S. HAO AND P.-G. MARTINSSON, *A direct solver for elliptic PDEs in three dimensions based on hierarchical merging of Poincaré–Steklov operators*, *Journal of Computational and Applied Mathematics*, 308 (2016), pp. 419–434, <https://doi.org/https://doi.org/10.1016/j.cam.2016.05.013>, <https://www.sciencedirect.com/science/article/pii/S0377042716302308>.
- [16] A. V. KNYAZEV, *Toward the optimal preconditioned eigensolver: Locally optimal block preconditioned conjugate gradient method*, *SIAM Journal on Scientific Computing*, 23 (2001), pp. 517–541, <https://doi.org/10.1137/S1064827500366124>, <https://doi.org/10.1137/S1064827500366124>, <https://arxiv.org/abs/https://doi.org/10.1137/S1064827500366124>.
- [17] M. KRONBICHLER AND K. KORMANN, *Fast matrix-free evaluation of discontinuous galerkin finite element operators*, *ACM Trans. Math. Softw.*, 45 (2019), <https://doi.org/10.1145/3325864>, <https://doi.org/10.1145/3325864>.
- [18] P. MARTINSSON, *A fast direct solver for a class of elliptic partial differential equations*, *Journal of Computational Physics*, 38 (2009), pp. 316–330, <https://doi.org/10.1007/s10915-008-9240-6>.
- [19] P. MARTINSSON, *A direct solver for variable coefficient elliptic PDEs discretized via a composite spectral collocation method*, *Journal of Computational Physics*, 242 (2013), pp. 460–479, <https://doi.org/https://doi.org/10.1016/j.jcp.2013.02.019>.
- [20] H. PFEIFFER, L. KIDDER, M. SCHEEL, AND S. TEUKOLSKY, *A multidomain spectral method for solving elliptic equations*, *Computer physics communications*, 152 (2003), pp. 253–273.
- [21] W. E. ROTH, *On direct product matrices*, *Bulletin of the American Mathematical Society*, 40 (1934), pp. 461 – 468, <https://doi.org/bams/1183497463>, <https://doi.org/>.
- [22] Y. SAAD AND M. H. SCHULTZ, *GMRES: A generalized minimal residual algorithm for solving nonsymmetric linear systems*, *SIAM Journal on Scientific and Statistical Computing*, 7 (1986), pp. 856–869, <https://doi.org/10.1137/0907058>, <https://doi.org/10.1137/0907058>,

- <https://arxiv.org/abs/https://doi.org/10.1137/0907058>.
- [23] E. SANCHEZ-PALENCIA, *Non-Homogeneous Media and Vibration Theory*, Lecture Notes in Physics, Springer-Verlag, Berlin, Heidelberg, 1980.
 - [24] B. F. SMITH, P. E. BJØRSTAD, AND W. D. GROPP, *Domain decomposition : parallel multilevel methods for elliptic partial differential equations*, Cambridge University Press, Cambridge, 1996.
 - [25] A. TOSELLI AND O. B. WIDLUND, *Domain decomposition methods : algorithms and theory*, Springer series in computational mathematics, Springer, Berlin, 2005.
 - [26] L. N. TREFETHEN, *Spectral Methods in MATLAB*, Society for Industrial and Applied Mathematics, 2000, <https://doi.org/10.1137/1.9780898719598>, <https://epubs.siam.org/doi/abs/10.1137/1.9780898719598>, <https://arxiv.org/abs/https://epubs.siam.org/doi/pdf/10.1137/1.9780898719598>.